Table 1: Mass spectrometry imaging data sets. AP-MALDI - Atmospheric Pressure Matrix Assisted Laser Desorption/Ionization, DESI - Desorption Electrospray Ionization, LAESI - Laser Ablation Electrospray Ionization, LTP - Low-temperature Plasma, Res. - lateral resolution, Tol. - mass tolerance. References: [1] (Oetjen *et al.* 2015), [2] (Zheng *et al.* 2020), [3] (Maldonado-Torres *et al.* 2014, 2017). [4] (Römpp *et al.* 2010, 2014).

Organism, tissue	**Technique**	**Res.** [µm]	**Tol.** [m/z]	**Dimensions**	**Pixels**
Human, colorectal cancer[1]	DESI (-)	100	± 0.3	67 × 64	4,288
Arabidopsis thaliana, leaf[2]	LAESI (-)	200	± 0.3	46 × 26	1,196
Chili, fruit[3]	LTP (+)	1000	± 0.3	85 × 50	4,250
Mouse, urinary bladder[4]	AP-MALDI (+)	10	± 0.1	260 × 134	34,860

The original DESI data set consists of four samples per image, which we separated for further processing.

We used the 'imzML' community data format (Schramm, Hester, Klinkert, Both, Heeren, Brunelle, Laprévote, Desbenoit, Robbe, Stoeckli, Spengler, and Römpp 2012; Römpp, Schramm, Hester, Klinkert, Both, Heeren, Stöckli, and Spengler 2011), which is used in many proprietary and open source programs for MSI data processing (Weiskirchen, Weiskirchen, Kim, and Winkler 2019). Several programs and workflows use the statistical language R, such as MSI.R (Gamboa-Becerra *et al.* 2015), Cardinal (Bemis *et al.* 2015), and the Galaxy MSI module (Föll, Moritz, Wollmann, Stillger, Vockert, Werner, Bronsert, Rohr, Grüning, and Schilling 2019). Recently, we published an R-based platform for MSI data processing with a graphical user interface, RmsiGUI (Rosas-Román, Ovando-Vázquez, Moreno-Pedraza, Guillén-Alonso, and Winkler 2020), which provides modules for the control of an open hardware imaging robot ('Open LabBot'), the processing of raw data, and the analysis of MSI data. We integrated the TrIQ algorithm into the RmsiGUI, but also provide the R code snippets to facilitate its adoption into other programs.

2.2. Threshold Intensity Quantization (TrIQ) Algorithm

An image is a function $f(x, y)$ that assigns an intensity level for each point x, y in a two-dimension space. In mass spectrometry imaging (MSI), $f(x, y)$ is related to the intensity of a single mass-to-charge (m/z) value; x and y depend on the lateral resolution of the instrument. For visualizing $f(x, y)$ on a computer screen or printer, the image must be digitized for both intensity and spatial coordinates; this process is termed quantization.

Intensity quantization transform a range of intensity values to a single discrete value called *gray level*. A common practice in intensity quantization is the use of equal spaced intensity bins k of width w:

$$w = \left\lceil \frac{H - L}{k} \right\rceil \tag{1}$$

H and L stand for the maximum and minimum intensity value of the image data, respectively.

The intensity quantization bins permit the building of an histogram $h(i)$, with i as the histogram bin index. The *Cumulative Distributive Function* (CDF) is defined as:

$$p(n) = \frac{\sum_{i=1}^{n} h(i)}{N}, \tag{2}$$

Where N represents the number of pixels within an image, and n any integer number between 1 to k.

The *Threshold Intensity Quantization*, or TrIQ, algorithm spots the upper limit T of the nth bin with the CDF closest to a given target probability P. Pixel intensities above the threshold T are grouped into the highest gray level. Remaining gray levels are quantized with the bin width given by equation (1), substituting H by T.

Depending on the raw data quality, the target probability P, and the number of bins k for computing T threshold and the final intensity quantification may be adjusted. From equation (2) follows that an increased k gives a better approximation of P. The default values for k and P in RmsiGUI are 100 and 98%, respectively.

2.3. Implementation

The algorithm was implemented in the programming language R (R Core Team 2018) and integrated into the graphical user interface of RmsiGUI (`https://bitbucket.org/lababi/rmsigui/`, Rosas-Román *et al.* (2020)).

Following, we explain an example R script for applying the TrIQ algorithm on an MSI data set step-by-step. The R script and the data set are provided as supplemental material of this article.

First, external R packages are loaded: The `viridis` color map, which is optimized for human perception and people with color vision deficiencies (Nuñez *et al.* 2018, Garnier, Ross, Rudis, Sciaini, and Scherer (2018)), and `MALDIquantForeign`, a package which enables the reading and processing of mass spectrometry imaging data (MSI) in imzML format (Gibb and Strimmer 2012, Gibb and Franceschi (2019)):

```
# ********************************************************************
# Loading external libraries
# ********************************************************************
if( is.loaded( "viridis" ) == FALSE )
  library( viridis )

if( is.loaded( "MALDIquantForeign" ) == FALSE )
  library( MALDIquantForeign )
```

Next, the main three functions implementing the TrIQ algorithm are defined: `GetOutlierThres`, `SetPixelDepth`, `Triq` and `GlobalTriq`.

The `GetOutlierThres` calculates an intensity range, which includes the majority of pixels. Typically, a value of 95 to 98 percent of the pixel intensities is chosen. Extreme intensity values are considered as outliers. When the image's intensity range exceeds 100 units, the

histogram is computed with 100 bins; otherwise, the number of bis is taken as the integer part of the intensity range.

```
# ************************************************************************
# TIQ Functions
# ************************************************************************

# Find intensity threshold closer to cumulative probability
#   source: Numeric matrix with image intensity
#     prob: Probability, 0.95-0.99 recommended
GetOutlierThres <- function( pixMap, prob ) {

  # Compute bins
  lim <- range( pixMap )

  if( lim[2] - lim[1] + 1 >= 100 ) {
    bins <- 100
    brk  <- seq(
      from       = lim[1],
      to         = lim[2] + ( lim[2] - lim[1] ) / ( bins - 1 ),
      length.out = bins+1 )
  }

  else {
    brk <- floor( lim[1] ):( ceiling( lim[2] ) + 1 )
  }

  # Compute histogram
  h <- hist( pixMap,
    breaks         = brk,
    right          = FALSE,
    include.lowest = FALSE,
    plot           = FALSE )

  # Get the bin closer to "prob"
  top   <- prob - cumsum( h$counts ) / sum( h$counts )
  delta <- abs( top )
  index <- 1 + which( min(delta) == delta )[1]

  # return range
  return( c( lim[1] , max( pixMap[ pixMap < h$breaks[index] ] ) ) )
}
```

`SetPixelDepth` performs the intensity quantization of the image. The intensity range is divided into equal bins, specified by the depth parameter.

```
# Adjust intensity dynamic range
```

```
#   pixMap: Input image
#   bounds: Intensity range on final image
#    depth: Number of gray levels
SetPixelDepth <- function( pixMap, bounds, depth ) {

  # Reserve memory for output matrix
  size     <- dim( pixMap )
  digital  <- matrix( 0, nrow=size[1], ncol=size[2] )

  # Compute bin Width
  binWidth <- ( depth - 1 ) / ( bounds[2] - bounds[1]  )
  value    <- c( 0, 0, depth - 1 )

  # Amplitude quantization
  for( i  in 1:length( pixMap ) ) {
    numb       <- ( pixMap[i] - bounds[1] ) * binWidth
    whole      <- trunc( numb )
    value[2]   <- whole - ( numb == whole )
    digital[i] <- value[ ( numb > 1 ) + ( pixMap[i] > bounds[2] ) + 1 ]
  }

  return( digital )
}
```

The `TrIQ` function uses the intensity range computed with `GetOutlierThres` to adjust the intensity range of an image.

```
# Remove pixel intensity outliers
#   pixMap: Input image
#    depth: Number of gray levels
TrIQ <- function( pixMap, depth, prob=0.98 ) {

  # Compute new dinamic range
  bounds <- GetOutlierThres( pixMap, prob )

  # Set intensity dinamyc range
  return( SetPixelDepth( pixMap, bounds, depth ) )
}
```

`GlobalTrIQ` applies the TrIQ procedure on a set of images for obtaining a comparable color scale among all processed images (see section 3.3).

```
# Apply TrIQ to a group of slices
#   slices: Slices list array
#    depth: Grey levels
#     prob: Target cumulative probability
GlobalTrIQ <- function( slices, depth, prob=0.98 ) {
```

```
  # Get intensity range
  bounds  <- range( sapply( slices, GetOutlierThres, prob ) )
  normImg <- lapply( slices, SetPixelDepth, bounds, depth )
  dim( normImg ) <- c( nrow( slices ), ncol( slices ) )

  # Display bounds
  print( bounds )

  # return normalization range
  return( normImg )
}
```

The auxiliary functions are necessary for data loading and visualization.

`GetSlice` extracts ion trace data, and `PlotSlices` is used for plotting ion images.

```
# ************************************************************************
# Auxiliary functions
# ************************************************************************

# Get slice from imzML object, set NAs to minimum value
#    mass: m/z value
#   imzML: Image object
#     tol: peak tolerance
GetSlice <- function( mass, imzML, tol ) {

  # Load Slice
  slice <- MALDIquant::msiSlices( imzML, center=mass, tolerance=tol )[,,1]

  # Set NA's
  index <- is.na( slice )
  if( length(index) ) {
    slice[ index ] <- min( slice, na.rm=TRUE )
  }

  return( slice )
}

PlotSlices <- function( slices, bins ) {

  # Set drawing options
  nRows <- nrow( slices )
  old   <- par(
    mfcol = c( nRows, ncol( slices ) ),
    mar   = c( 0.2,0.2,0.2,0.2 ) )

  # Draw slices
```

```
  lapply( slices, function(x)
    image( x, asp=ncol(x)/nrow(x), axes=FALSE,
           col=viridis( bins ) ) )

  # Restore options
  par( old )
}
```

The `MedianFilter` function may be used to remove technical noise, such as random intensity spikes.

```
# Median Filter with 3x3 mask
#   pixMap: input image
MedianFilter <- function( pixMap ) {

  width  <- ncol(pixMap)
  height <- nrow(pixMap)

  target <- matrix( 0, nrow=height, ncol=width )

  for( j in 2:(width-1) ) {
    for( i in 2:(height-1) ) {
      index <- (i-1):(i+1)
      target[i,j] <- median( c(
        pixMap[ index, j-1 ],
        pixMap[ index, j ],
        pixMap[ index, j+1 ] ) )
    }
  }

  return( target )
}
```

The following code demonstrates the processing of an imzML dataset with the next steps: loading the data, extracting ion traces of interest, TrIQ normalization, and median filtering. Unprocessed images, the TrIQ normalized, and the median-filtered images are plotted, as shown in Figure 5.

```
# ******************************************************************
# Processing of the dataset ltpmsi-chilli.imzML
# ******************************************************************
chili <- import( "./ltpmsi-chilli.imzML" )

# Get slices
imgList <- lapply( c(62.1, 84.1, 306.1 ), GetSlice, chili, 0.3 )
dim( imgList ) <- c(3, 1)
PlotSlices( imgList, 256 )
```

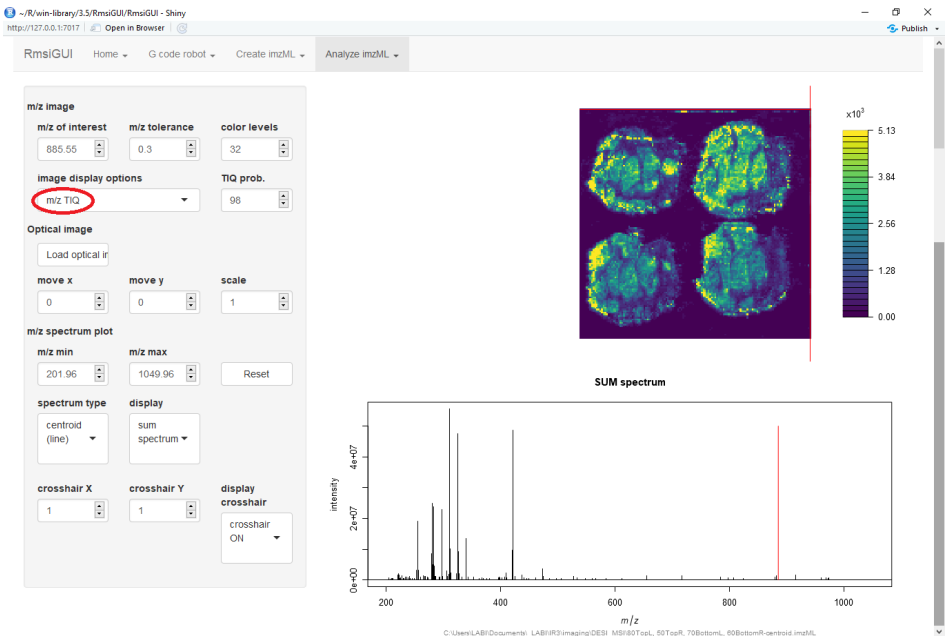

Figure 1: Implementation of the Threshold Intensity Quantization (TrIQ) in the graphical user interface RmsiGUI.

```
# Normalize with TrIQ
lev <- 5
norList <- GlobalTrIQ( imgList, lev, 0.98 )
PlotSlices( norList, lev )

# Median filter
medList <- lapply( norList, MedianFilter )
dim( medList ) <- dim( imgList )
PlotSlices( medList, lev )
```

Figure 1 shows the graphical user interface of RmsiGUI with the TrIQ option selector.

3. Results and discussion

For plotting data, R applies an intensity quantization by default. The image features can be enhanced by additional operations, such as global or local histogram equalization algorithms; however, such an image processing does not preserve the linearity of the original gray level scale.

In contrast, our approach finds an intensity threshold of T for saturating the last gray level of the image. Therefore the linearity of the experimentally determined intensity scale is preserved. In the next sections, we demonstrate the application of the Threshold Intensity

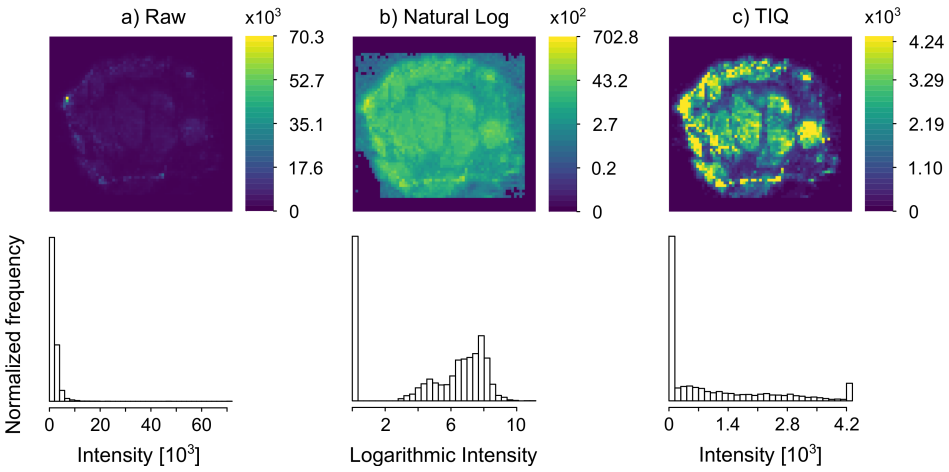

Figure 2: Contrast enhancement by Threshold Intensity Quantization (TrIQ). The mass trace 885.55 *m/z* of DESI MSI data of a human colorectal adenocarcinoma sample was visualized with different quantization methods. a) Raw data, rendered with 256 gray levels. b) Plotting with applying the natural logarithm to the intensity values. c) Image contrast improvement after TrIQ with 95 percent and 32 gray levels. All the histograms were computed with 32 bins.

Quantization (TrIQ) for the processing of mass spectrometry imaging (MSI) datasets.

3.1. Contrast optimization

Figure 2 shows the mass spectrometry image of a human colorectal adenocarcinoma sample, acquired with DESI and 100 μm spatial resolution (Oetjen *et al.* 2015). The imaged signal of 885.55 *m/z,* corresponds to de-protonated phosphatidylinositol (18:0/20:4), $[C_{47}H_{83}O_{13}P\text{-}H]^-$ (Tillner, Wu, Jones, Pringle, Karancsi, Dannhorn, Veselkov, McKenzie, and Takats 2017).

The direct plotting of the extracted *m/z* slice results in the image shown in Figure 2a). The image contains pixels with intensity values up 70,280 arbitrary units. Such extreme and infrequent intensity values are called *outliers* and drastically reduce image contrast. The histogram below Figure 2a) reveals the reason for the low contrast of the image: Most of the pixels fall into the first four bins after the standard intensity quantization.

A typical data transformation for imaging is the use of a logarithmic intensity scale. Figure 2b) shows the resulting image after applying the natural logarithm in Figure 2b). The contrast is improved. However, further operations would be necessary, such as the subtraction of the background level. Besides, the interpretation of the non-linear color scale less intuitive.

Applying the TrIQ algorithm with $P = 0.95$ results in Figure 2c). Pixels with intensities above $T = 4,244$ are binned within the highest gray level. The corresponding histogram shows an almost flat frequency over a wide intensity range. Compared to the unprocessed image, the contrast of the image is drastically improved, and the linear intensity scale of the color representation is preserved.

3.2. Background optimization

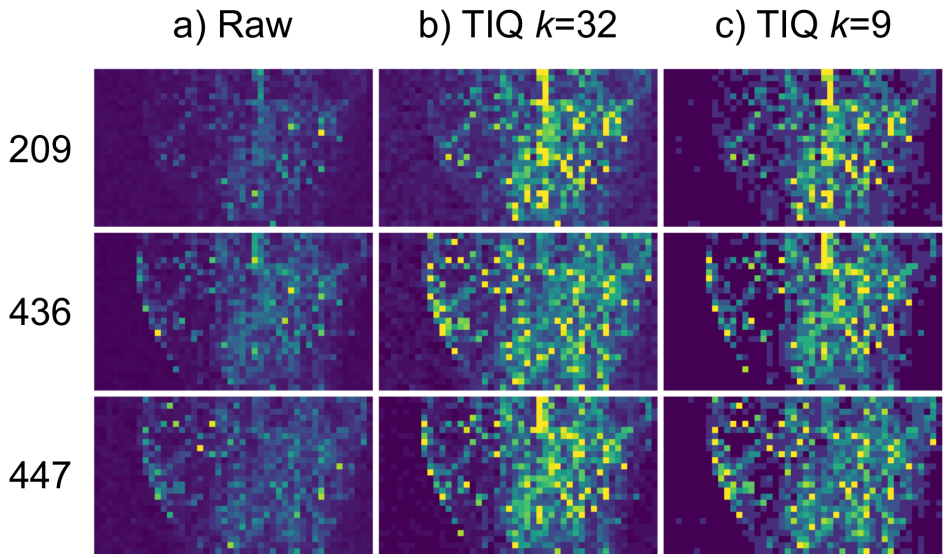

Figure 3: Background optimization with TrIQ. Three mass traces of LAESI MSI data from *Arabidopsis thaliana* are plotted. a) Raw data plotting with 256 gray levels b) TrIQ with 32 gray applied, c) TrIQ with 9 gray levels. The background uniformity is improved by reducing the intensity and gray levels.

The number of gray levels used for intensity quantization has an impact on the quality of the processed image, for example, its background noise. Figure 3 shows the rendering of signals from an *Arabidopsis thaliana* leaf, analyzed by LAESI MSI with a lateral resolution of 200 μm (Zheng *et al.* 2020). The images correspond to the negative ions of the putative ions of 4-hydroxymethyl-3-methoxyphenoxyacetic acid ($[C_{10}H_{12}O_5\text{-}3H]^-$, 209.0 m/z), 4-methylsulfonylbutyl glucosinolate ($[C_{12}H_{23}NO_{10}S_3\text{-}H]^-$, 436.0 m/z), and indol-3-ylmethyl glucosinolate ($[C_{16}H_{20}N_2O_9S_2\text{-}H]^-$, 447.1 *m/z*)(Wu, Tohge, Cuadros-Inostroza, Tong, Tenenboim, Kooke, Méret, Keurentjes, Nikoloski, Fernie, Willmitzer, and Brotman 2018).

Comparing Figures 3a) and 3b) illustrates that removing outliers with TrIQ and reducing gray levels lead to an improvement of the image brightness. Nevertheless, the background still appears noisy, and the sample shape is not well defined yet. Reducing the gray levels from 32 to 9 results in an almost perfectly uniform background and a well-defined sample shape, as shown in Figure 3c).

Consequently, the TrIQ algorithm can be applied to detect a sample mask for background subtraction, as demonstrated in section 3.4.

3.3. Normalization for comparable mass spectrometry images

Comparing mass spectrometry images (MSI) is a challenge because they usually display distinct intensity and color scales. TrIQ can be applied to a group of images and normalize their intensity ranges.

Figure 4 shows human colorectal adenocarcinoma images. The samples come from the same tissue, which was cut to slices with a thickness of 10 μm (Oetjen *et al.* 2015). All images visualize the abundance of the ion 885.55 *m/z*. A maximum threshold T of 4,970 was calculated and applied for all twelve images; the accumulated probability was set to 0.91. The resulting

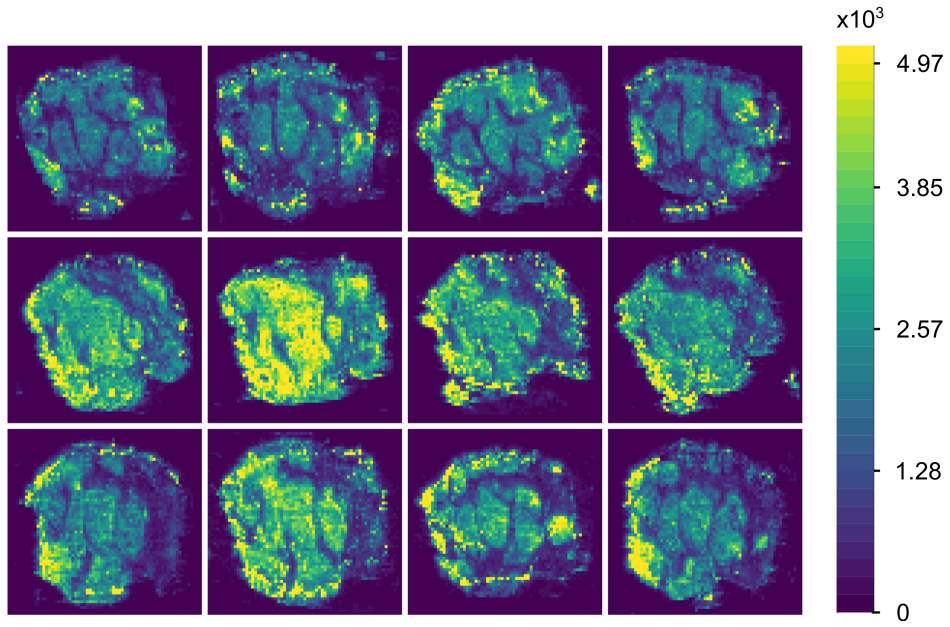

Figure 4: Global TrIQ applied to the ion 885.55 m/z of human colorectal adenocarcinoma DESI MSI slices, with P = 0.91 and 32 gray levels. The normalization allows a direct comparison of the images.

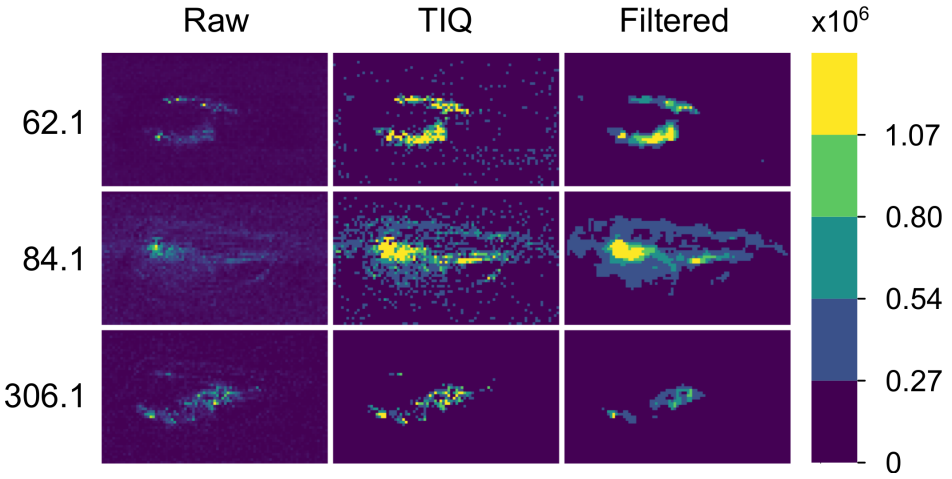

Figure 5: LTP MSI of a chili *Capsicum annuum* fruit with 1 mm lateral resolution. TrIQ with P = 0.98 and 5 gray levels improves the contrast; an additional median filter removes technical noise.

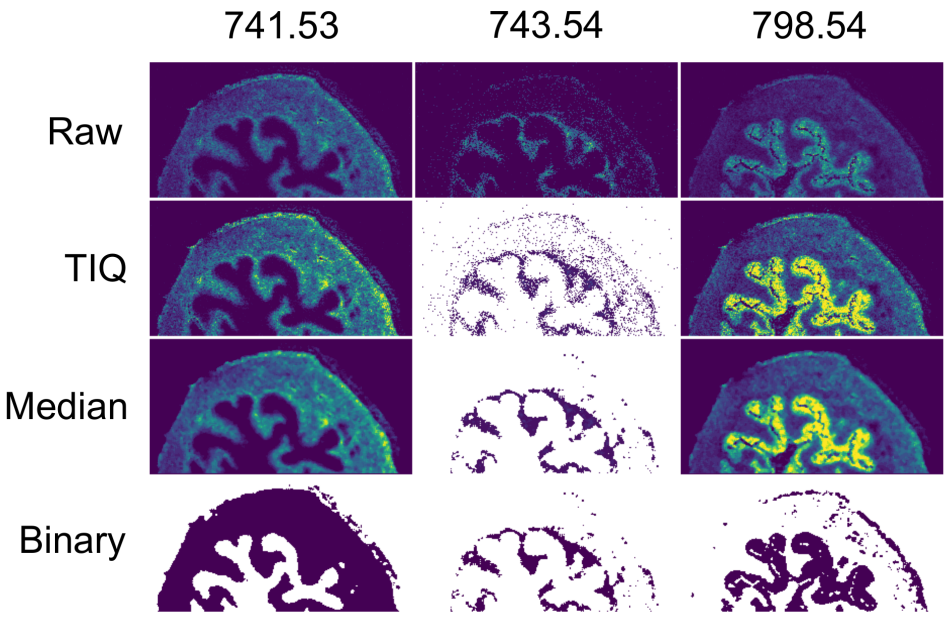

Figure 6: AP-MALDI MSI of a mouse urinary bladder imaged with a lateral resolution of 10 µm. TrIQ was applied with P = 0.95 and 25 gray levels. Binary images serve for defining regions of interest (ROI) and segmentation: 741.53 *m/z* - muscle tissue, 743.54 *m/z* - *lamina propria* structure, 798.54 *m/z* - *urothelium*.

color scale is the same for all images. Thus, the relative abundance and distribution of an ion of multiple images can be evaluated at a single glance.

Figure 5 provides another example of global TrIQ. The image compares the 62.1, 84.1, and 306.1 *m/z* ions of chili (*Capsicum annuum)* slices sampled at 1 mm lateral resolution with low-temperature plasma (LTP) MSI (Maldonado-Torres *et al.* 2014). LTP MSI detects small, volatile compounds. Therefore, the images resulting from this ambient ionization method are noisy. TrIQ with $P = 0.98$ and five gray levels improved the contrast. The remaining noise is efficiently removed with a 3×3 median filter, as illustrated in Figure 5. The signals with a mass-to-charge ratio of 62.1 and 84.1 display a defined localization at the seeds and in at the center of the placenta, respectively. The signal with 306.1 *m/z* is enriched in placenta tissue and corresponds to the $[C_{18}H_{27}NO_3{+}H]^+$ ion of capsaicin, the compound responsible for the hot taste of chili peppers (Aza-González, Núñez-Palenius, and Ochoa-Alejo 2011; Maldonado-Torres *et al.* 2014; Gamboa-Becerra *et al.* 2015; Cervantes-Hernández, Alcalá-González, Martínez, and Ordaz-Ortiz 2019).

Both examples demonstrate the usefulness of TrIQ to normalize MSI data for comparing images.

3.4. Image segmentation for visualizing regions of interest (ROI)

The combination of global TrIQ and median filtering can be expanded for image segmentation. Figure 6 was obtained from a mouse urinary bladder, scanned using AP-MALDI MSI at a lateral resolution of 10 μm (Römpp *et al.* 2010, 2014). The distribution of 741.53 *m/z*, identified as a sphingomyelin $[C_{39}H_{79}N_2O_6P + K]^+$ ion, is related to muscle tissue. 743.54

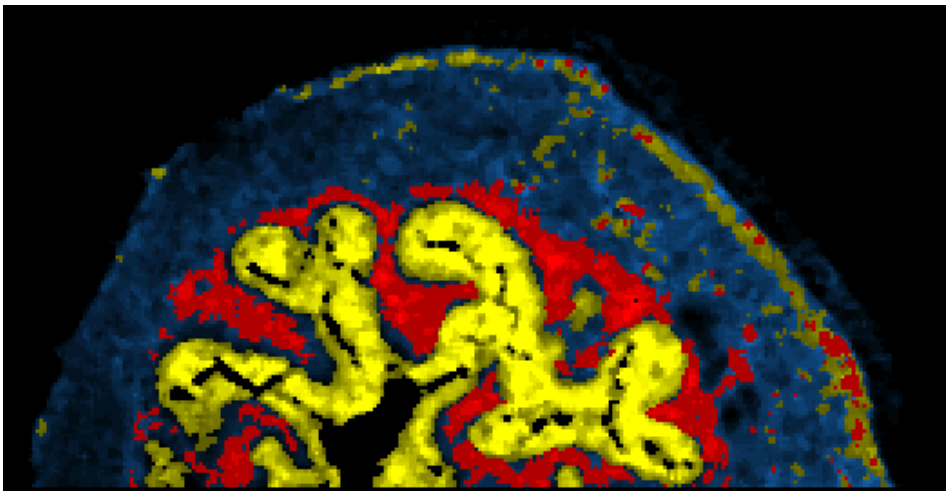

Figure 7: Overlay image, representing the anatomical structures in mouse urinary bladder. Blue: 741.53 *m/z* - muscle tissue, red: 743.54 *m/z* - *lamina propria* , yellow: 798.54 *m/z* - *urothelium*.

m/z is associated with the *lamina propria* structure, while 798.54 *m/z* is mainly found in the *urothelium* (Römpp *et al.* 2010). Global TrIQ was applied with $P = 0.95$ and 25 gray levels.

TrIQ and median filtering allow clear discrimination between muscle tissue and *lamina propria* using the marker ions 741.53 and 743.54 *m/z*. *For separating t*he *urothelium* structure from the muscular tissue, the binary image for 798.54 *m/z* was calculated by zeroing gray levels below 9.

Figure 7 shows an overlay of the resulting ion images, representing correctly the anatomical structures of the mouse urinary bladder.

3.5. Computational performance of algorithm

For estimating the computational performance of the TrIQ algorithm, we reprocessed selected ion traces presented in this paper (DESI 885.55 *m/z*, LAESI 209 *m/z*, LTP 62.1 *m/z* and AP-MALDI 741.53 *m/z*) and measured the time for applying the TrIQ. The calculation was executed for twenty-five times to account for variations in system processes of the operating system. Figure 8 demonstrates the results from running the R script `Timing.R` (provided as supplemental code) on a standard Linux laptop (Intel(R) Core(TM) i7-7700HQ CPU with 2.80GHz, 16 Gb RAM, Peppermint OS 10). On average, more than 1,000 pixels were processed per millisecond. Thus, TrIQ is computationally efficient, and also exhibited comparable performance with MSI datasets of different sizes, proving the scalability of the algorithm.

4. Conclusions

Threshold Intensity Optimization (TrIQ) improves the visualization of mass spectrometry imaging (MSI) data by augmenting the contrast and homogenizing the background. Contrary to histogram equalization algorithms, TrIQ preserves the linearity of measured ion intensities. The processing with TrIQ facilitates the recognition of regions of interest (ROI) in MSI

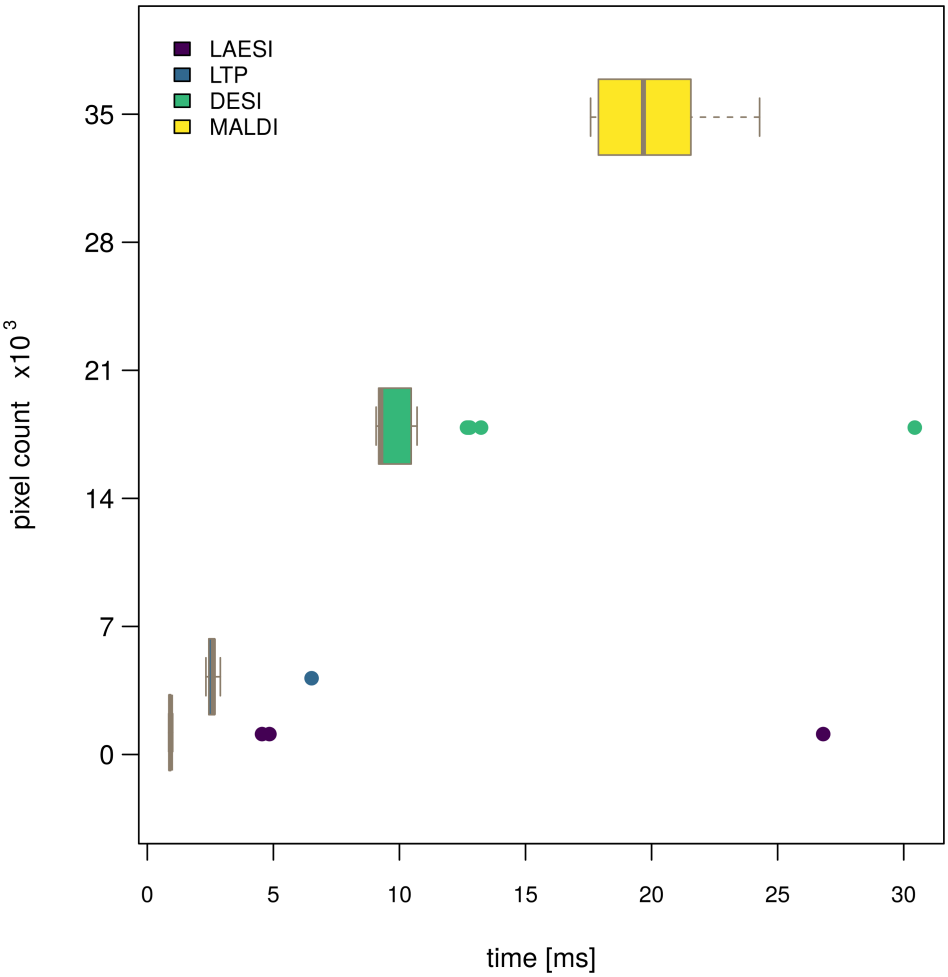

Figure 8: Execution speed of the TrIQ algorithm, implemented in R, using a standard laptop.

data sets, either by visual inspection of by automated segmentation algorithms and therefore supports the interpretation of MSI data in biology and medicine.
Applying TrIQ to a set of images equalizes their intensity scales, and makes them comparable. We demonstrated the implementation of the TrIQ algorithms in R for the processing of MSI data in the community format imzML. The algorithm is computationally fast and only requires basic operations, and thus can be quickly adapted to any programming language.
TrIQ can be applied to improve the plotting of any scientific data with extreme values, respecting the original intensity levels of raw data.

5. Code availability

The R code for reproducing the results of this article is provided as supplemental material. RmsiGUI is freely available from https://bitbucket.org/lababi/rmsigui/. We released TrIQ R scripts and the R package RmsiGUI under the terms of the GNU General Public License, GPL V3 (http://gplv3.fsf.org/).

6. Acknowledgments

We thank Dr. Abigail Moreno Pedraza, Dr. Teresa Maria Teresa Carrillo Rayas, Maria Isabel Cristina Elizarraraz Anaya, and Thermo Mexico for technical support. The project was funded by the CONACyT bilateral grant CONACyT-DFG 2016/277850. IRR acknowledges his CONACyT PostDoc scholarship.

7. Conflicts of interest

RW is the co-inventor of the patent application "Non-thermal plasma jet device as source of spatial ionisation for ambient mass spectrometry and method of application" (WO 2014/057409) and a shareholder of the company Kuturabi SA de CV.

8. Author contributions

Conceptualization: IRR, RW; Data curation: IRR, RW; Formal Analysis: IRR; Funding acquisition: RW; Investigation: IRR; Methodology: IRR; Project administration: RW; Resources: RW; Software: IRR; Supervision: RW; Validation: IRR, RW; Visualization: IRR; Writing – original draft: IRR, RW; Writing – review & editing: RW;

References

Abdullah-Al-Wadud M, Kabir MH, Akber Dewan MA, Chae O (2007). "A Dynamic Histogram Equalization for Image Contrast Enhancement." *IEEE Transactions on Consumer Electronics*, **53**(2), 593–600. ISSN 1558-4127. doi:10.1109/TCE.2007.381734.

Aza-González C, Núñez-Palenius HG, Ochoa-Alejo N (2011). "Molecular biology of capsai-

cinoid biosynthesis in chili pepper (Capsicum spp.)." *Plant cell reports*, **30**(5), 695–706. ISSN 1432-203X. doi:10.1007/s00299-010-0968-8.

Bemis KD, Harry A, Eberlin LS, Ferreira C, van de Ven SM, Mallick P, Stolowitz M, Vitek O (2015). "Cardinal: an R package for statistical analysis of mass spectrometry-based imaging experiments." *Bioinformatics (Oxford, England)*. ISSN 1367-4811. doi:10.1093/bioinformatics/btv146.

Borland D, Taylor Ii RM (2007). "Rainbow Color Map (Still) Considered Harmful." *IEEE Computer Graphics and Applications*, **27**(2), 14–17. ISSN 1558-1756. doi:10.1109/MCG.2007.323435.

Cervantes-Hernández F, Alcalá-González P, Martínez O, Ordaz-Ortiz JJ (2019). "Placenta, Pericarp, and Seeds of Tabasco Chili Pepper Fruits Show a Contrasting Diversity of Bioactive Metabolites." *Metabolites*, **9**(10), 206. doi:10.3390/metabo9100206. Number: 10 Publisher: Multidisciplinary Digital Publishing Institute, URL https://www.mdpi.com/2218-1989/9/10/206.

Doi K (2006). "Diagnostic imaging over the last 50 years: research and development in medical imaging science and technology." *Physics in Medicine and Biology*, **51**(13), R5–R27. ISSN 0031-9155. doi:10.1088/0031-9155/51/13/R02. URL https://doi.org/10.1088%2F0031-9155%2F51%2F13%2Fr02.

Föll MC, Moritz L, Wollmann T, Stillger MN, Vockert N, Werner M, Bronsert P, Rohr K, Grüning BA, Schilling O (2019). "Accessible and reproducible mass spectrometry imaging data analysis in Galaxy." *GigaScience*, **8**(12). ISSN 2047-217X. doi:10.1093/gigascience/giz143.

Gamboa-Becerra R, Ramírez-Chávez E, Molina-Torres J, Winkler R, Ramírez-Chávez E, Molina-Torres J, Winkler R (2015). "MSI.R scripts reveal volatile and semi-volatile features in low-temperature plasma mass spectrometry imaging (LTP-MSI) of chilli (Capsicum annuum)." *Analytical and Bioanalytical Chemistry*, **407**(19), 5673–5684. doi:10.1007/s00216-015-8744-9. URL http://link.springer.com/10.1007/s00216-015-8744-9.

Garnier S, Ross N, Rudis B, Sciaini M, Scherer C (2018). "viridis: Default Color Maps from 'matplotlib'." URL https://CRAN.R-project.org/package=viridis.

Gibb S, Franceschi P (2019). "MALDIquantForeign: Import/Export Routines for 'MALDIquant'." URL https://CRAN.R-project.org/package=MALDIquantForeign.

Gibb S, Strimmer K (2012). "MALDIquant: a versatile R package for the analysis of mass spectrometry data." *Bioinformatics*, **28**(17), 2270–2271. ISSN 1367-4803, 1460-2059. doi:10.1093/bioinformatics/bts447. URL http://bioinformatics.oxfordjournals.org/content/28/17/2270.

Gomès S, Assy A, Chapuis PO (2015). "Scanning thermal microscopy: A review." *physica status solidi (a)*, **212**(3), 477–494. ISSN 1862-6319. doi:10.1002/pssa.201400360. URL https://onlinelibrary.wiley.com/doi/abs/10.1002/pssa.201400360.

Gormanns P, Reckow S, Poczatek JC, Turck CW, Lechene C (2012). "Segmentation of Multi-Isotope Imaging Mass Spectrometry Data for Semi-Automatic Detection of Regions

of Interest." *PLOS ONE*, **7**(2), e30576. ISSN 1932-6203. doi:10.1371/journal.pone.0030576. URL https://journals.plos.org/plosone/article?id=10.1371/journal.pone.0030576.

Kimpe T, Tuytschaever T (2007). "Increasing the Number of Gray Shades in Medical Display Systems—How Much is Enough?" *Journal of Digital Imaging*, **20**(4), 422–432. ISSN 1618-727X. doi:10.1007/s10278-006-1052-3. URL https://doi.org/10.1007/s10278-006-1052-3.

López-Fernández H, Santos HM, Capelo JL, Fdez-Riverola F, Glez-Peña D, Reboiro-Jato M (2015). "Mass-Up: an all-in-one open software application for MALDI-TOF mass spectrometry knowledge discovery." *BMC Bioinformatics*, **16**(1), 318. ISSN 1471-2105. doi:10.1186/s12859-015-0752-4. URL https://doi.org/10.1186/s12859-015-0752-4.

Lu H, Zhang H, Chingin K, Xiong J, Fang X, Chen H (2018). "Ambient mass spectrometry for food science and industry." *TrAC Trends in Analytical Chemistry*, **107**, 99–115. ISSN 0165-9936. doi:10.1016/j.trac.2018.07.017. URL http://www.sciencedirect.com/science/article/pii/S0165993618302814.

Maldonado-Torres M, López-Hernández JF, Jiménez-Sandoval P, Winkler R (2014). "'Plug and Play' assembly of a low-temperature plasma ionization mass spectrometry imaging (LTP-MSI) system." *Journal of proteomics*, **102C**, 60–65. doi:10.1016/j.jprot.2014.03.003. URL http://linkinghub.elsevier.com/retrieve/pii/S1874391914001250.

Maldonado-Torres M, López-Hernández JF, Jiménez-Sandoval P, Winkler R (2017). "Low-temperature plasma mass spectrometry imaging (LTP-MSI) of Chili pepper." doi:10.5281/zenodo.484496. Type: dataset, URL https://zenodo.org/record/484496#.XnpM7tHPxhE.

Nuñez JR, Anderton CR, Renslow RS (2018). "Optimizing colormaps with consideration for color vision deficiency to enable accurate interpretation of scientific data." *PLOS ONE*, **13**(7), e0199239. ISSN 1932-6203. doi:10.1371/journal.pone.0199239. URL https://journals.plos.org/plosone/article?id=10.1371/journal.pone.0199239.

Oetjen J, Veselkov K, Watrous J, McKenzie JS, Becker M, Hauberg-Lotte L, Kobarg JH, Strittmatter N, Mróz AK, Hoffmann F, Trede D, Palmer A, Schiffler S, Steinhorst K, Aichler M, Goldin R, Guntinas-Lichius O, von Eggeling F, Thiele H, Maedler K, Walch A, Maass P, Dorrestein PC, Takats Z, Alexandrov T (2015). "Benchmark datasets for 3D MALDI- and DESI-imaging mass spectrometry." *GigaScience*, **4**. ISSN 2047-217X. doi:10.1186/s13742-015-0059-4. URL https://www.ncbi.nlm.nih.gov/pmc/articles/PMC4418095/.

R Core Team (2018). *R: A Language and Environment for Statistical Computing*. R Foundation for Statistical Computing, Vienna, Austria. URL https://www.R-project.org/.

Race AM, Bunch J (2015). "Optimisation of colour schemes to accurately display mass spectrometry imaging data based on human colour perception." *Analytical and Bioanalytical Chemistry*, pp. 1–8. ISSN 1618-2642, 1618-2650. doi:10.1007/s00216-014-8404-5. URL http://link.springer.com/article/10.1007/s00216-014-8404-5.

Rae Buchberger A, DeLaney K, Johnson J, Li L (2018). "Mass Spectrometry Imaging: A Review of Emerging Advancements and Future Insights." *Analytical chemistry*, **90**(1), 240–265. ISSN 0003-2700. doi:10.1021/acs.analchem.7b04733. URL https://www.ncbi.nlm.nih.gov/pmc/articles/PMC5959842/.

Rogowitz BE, Treinish LA, Bryson S (1996). "How Not to Lie with Visualization." *Computers in Physics*, **10**, 268. ISSN 0894-1866. URL http://adsabs.harvard.edu/abs/1996ComPh..10..268R.

Römpp A, Guenther S, Schober Y, Schulz O, Takats Z, Kummer W, Spengler B (2010). "Histology by Mass Spectrometry: Label-Free Tissue Characterization Obtained from High-Accuracy Bioanalytical Imaging." *Angewandte Chemie International Edition*, **49**(22), 3834–3838. ISSN 1521-3773. doi:10.1002/anie.200905559. URL https://onlinelibrary.wiley.com/doi/abs/10.1002/anie.200905559.

Römpp A, Guenther S, Schober Y, Schulz O, Takats Z, Kummer W, Spengler B (2014). "ProteomeXchange Dataset PXD001283." URL http://proteomecentral.proteomexchange.org/cgi/GetDataset?ID=PXD001283.

Römpp A, Schramm T, Hester A, Klinkert I, Both JP, Heeren RMA, Stöckli M, Spengler B (2011). "imzML: Imaging Mass Spectrometry Markup Language: A common data format for mass spectrometry imaging." *Methods in molecular biology (Clifton, N.J.)*, **696**, 205–224. ISSN 1940-6029. doi:10.1007/978-1-60761-987-1_12.

Rosas-Román I, Ovando-Vázquez C, Moreno-Pedraza A, Guillén-Alonso H, Winkler R (2020). "Open LabBot and RmsiGUI: Community development kit for sampling automation and ambient imaging." *Microchemical Journal*, **152**, 104343. ISSN 0026-265X. doi:10.1016/j.microc.2019.104343. URL http://www.sciencedirect.com/science/article/pii/S0026265X19321873.

Schramm T, Hester A, Klinkert I, Both JP, Heeren RMA, Brunelle A, Laprévote O, Desbenoit N, Robbe MF, Stoeckli M, Spengler B, Römpp A (2012). "imzML - a common data format for the flexible exchange and processing of mass spectrometry imaging data." *Journal of proteomics*, **75**(16), 5106–5110. ISSN 1876-7737. doi:10.1016/j.jprot.2012.07.026.

Stauffer R, Mayr GJ, Dabernig M, Zeileis A (2014). "Somewhere over the rainbow: How to make effective use of colors in meteorological visualizations." *Bulletin of the American Meteorological Society*. ISSN 0003-0007. doi:10.1175/BAMS-D-13-00155.1. URL http://journals.ametsoc.org/doi/abs/10.1175/BAMS-D-13-00155.1.

Stockham T (1972). "Image processing in the context of a visual model." *Proceedings of the IEEE*, **60**(7), 828–842. ISSN 1558-2256. doi:10.1109/PROC.1972.8782.

Tillner J, Wu V, Jones EA, Pringle SD, Karancsi T, Dannhorn A, Veselkov K, McKenzie JS, Takats Z (2017). "Faster, More Reproducible DESI-MS for Biological Tissue Imaging." *Journal of the American Society for Mass Spectrometry*, **28**(10), 2090–2098. ISSN 1879-1123. doi:10.1007/s13361-017-1714-z.

Weiskirchen R, Weiskirchen S, Kim P, Winkler R (2019). "Software solutions for evaluation and visualization of laser ablation inductively coupled plasma mass spectrometry

imaging (LA-ICP-MSI) data: a short overview." *Journal of Cheminformatics*, **11**(1), 16. ISSN 1758-2946. doi:10.1186/s13321-019-0338-7. URL https://doi.org/10.1186/s13321-019-0338-7.

Winkler R (2015). "An evolving computational platform for biological mass spectrometry: workflows, statistics and data mining with MASSyPup64." *PeerJ*, **3**(e1401), 1–34. ISSN 2167-8359. doi:10.7717/peerj.1401.

Wu S, Tohge T, Cuadros-Inostroza Á, Tong H, Tenenboim H, Kooke R, Méret M, Keurentjes JB, Nikoloski Z, Fernie AR, Willmitzer L, Brotman Y (2018). "Mapping the Arabidopsis Metabolic Landscape by Untargeted Metabolomics at Different Environmental Conditions." *Molecular Plant*, **11**(1), 118–134. ISSN 1674-2052. doi:10.1016/j.molp.2017.08.012. URL http://www.sciencedirect.com/science/article/pii/S1674205217302423.

Zeileis A, Hornik K, Murrell P (2009). "Escaping RGBland: Selecting colors for statistical graphics." *Computational Statistics & Data Analysis*, **53**(9), 3259–3270. ISSN 0167-9473. doi:10.1016/j.csda.2008.11.033. URL http://www.sciencedirect.com/science/article/pii/S0167947308005549.

Zheng Z, Bartels B, Svatoš A (2020). "Laser Ablation Electrospray Ionization Mass Spectrometry Imaging (LAESI MSI) of Arabidopsis thaliana leaf." doi:10.5281/zenodo.3678473. Type: dataset, URL https://zenodo.org/record/3678473#.XnpMu9HPxhE.

Affiliation:

Ignacio Rosas-Román
Center for Research and Advanced Studies (CINVESTAV) Irapuato
Department of Biochemistry and Biotechnology
Km. 9.6 Libramiento Norte Carr. Irapuato-León
36824 Irapuato Gto., Mexico
E-mail: ignacio.rosas@cinvestav.mx

Robert Winkler
Center for Research and Advanced Studies (CINVESTAV) Irapuato
Department of Biochemistry and Biotechnology
Km. 9.6 Libramiento Norte Carr. Irapuato-León
36824 Irapuato Gto., Mexico
E-mail: robert.winkler@cinvestav.mx
URL: http://www.ira.cinvestav.mx/lababi.aspx